Bioorganic Chemistry 92 (2019) 103219

Contents lists available at ScienceDirect

Bioorganic Chemistry

journal homepage: www.elsevier.com/locate/bioorg

Synthesis, anticancer activity and molecular docking studies on 1,2-diarylbenzimidazole analogues as anti-tubulin agents

Ya-Liang Zhang[a,1], Rong Yang[a,1], Lin-Ying Xia[a], Ruo-Jun Man[a,b], Yi-Chun Chu[a], Ai-Qin Jiang[c,*], Zhong-Chang Wang[a,*], Hai-Liang Zhu[a,*]

[a] State Key Laboratory of Pharmaceutical Biotechnology, School of Life Sciences, Nanjing University, Nanjing 210023, People's Republic of China
[b] Guangxi Biological Polysaccharide Separation, Purification and Modification Research Platform, Guangxi University for Nationalities, Nanning 530006, People's Republic of China
[c] Medical School, Nanjing University, Nanjing 210093, People's Republic of China

ARTICLE INFO

Keywords:
Tubulin inhibitor
Benzimidazole
Cell cycle arrest
Apoptosis
Molecular docking

ABSTRACT

Twenty-four 1,2-diarylbenzimidazole derivatives were designed, synthesized and biologically evaluated. It turned out that most of them were potential anticancer drugs. Among them, compound **c24** showed the highest anti-tumor activity (GI_{50} = 0.71–2.41 μM against HeLa, HepG2, A549 and MCF-7 cells), and low toxicity to normal cells (CC_{50} > 100 μM against L02 cells). In the microtubule binding assay, **c24** showed the most potent inhibition of microtubule polymerization (IC_{50} = 8.47 μM). The binding ability of compound **c24** to tubulin crystal was verified by molecular docking simulation experiment. Further studies on HepG2 and HeLa cells showed that compound **c24** could cause mitotic arrest of tumor cells to G2/M phase then inducing apoptosis. To sum up, compound **c24** is a promising microtubule assembly inhibitor.

1. Introduction

The incidence of cancer in China is on the rise year by year, so it is urgent to develop more effective cancer prevention and treatment programs [1]. Malignant tumor is a kind of disease with unlimited cell proliferation and abnormal differentiation, while chemotherapy drugs have the effect of "cytotoxicity" and promoting differentiation, which can kill cancer cells [2]. Chemotherapy, as a main treatment method, plays an increasingly important role in the overall comprehensive treatment. It is not only suitable for advanced [3] and recurrent cases [4], but also plays a role in the treatment of early patients.

Microtubules are composed of tubulin and microtubule binding protein, which are the main components of cytoskeleton [5]. Microtubules have the kinetic properties of polymerization and depolymerization, whose key functions are maintaining cell morphology, cell division and proliferation, organelle composition and transport, and signaling material transmission [6,7]. Anti-cancer drugs targeting microtubules use their kinetic properties to either promote or inhibit their polymerization [8]. Studies have shown that there are three mainly different inhibitory binding sites on tubulin: paclitaxel site, vincristine site and colchicine site [9,10]. Due to the small volume of the colchicine site cavity and the simple structure of the corresponding inhibitor, the research on its inhibitor has attracted much attention in recent years [11,12].

Combretastatin A-4 (CA-4, Fig. 1) was a product originally isolated from the *Combretum caffrum* in South Africa [13]. The structure-activity relationship showed that the *cis*-configuration of two aromatic rings and the three methoxy groups of A-ring were important pharmacores for the strong anti-cancer activity of CA-4 [14]. However, *cis*-double bonds in CA-4 structure were easy to be isomerized into more stable *trans*-double bonds in thermokinetics during the process of preservation and use, thus reducing the activity [15,16]. Therefore, many researches have been devoted to replacing the *cis*-double bond of CA-4 with different rigid linkers including heterocyclic ring systems to avoid the problem of structural isomerization of CA-4 [17,18]. Meanwhile, the B-ring of CA-4 was changed to obtain CA-4 analogues with better pharmacodynamics and pharmacokinetics characteristics. The structure of the designed compound was modified to replace the double bond of CA-4 with heterocyclic ring, which not only stabilized the *cis*-configuration but also improved the stability of the compound.

Benzimidazole was one of the earliest nitrogen-containing heterocyclic compounds [19], whose structure as a kind of dominant framework had been widely studied in the field of pharmacy. Compounds containing benzimidazole had a wide range of biological activities, such

* Corresponding authors.
E-mail addresses: jianaq@nju.edu.cn (A.-Q. Jiang), wangzhongchang2006@163.com (Z.-C. Wang), zhuhl@nju.edu.cn (H.-L. Zhu).
[1] These authors equally contributed to this paper.

https://doi.org/10.1016/j.bioorg.2019.103219
Received 27 January 2019; Received in revised form 11 July 2019; Accepted 24 August 2019
Available online 26 August 2019
0045-2068/

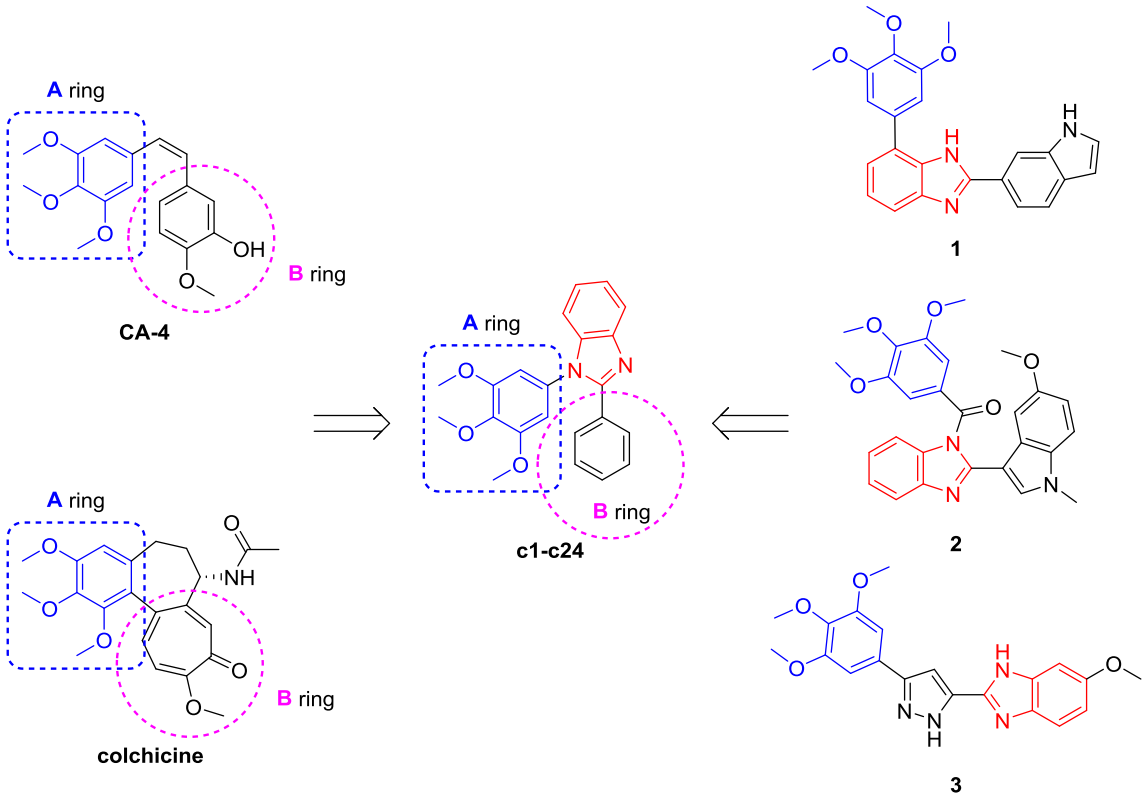

Fig. 1. Structure of reference and target compounds.

as anti-inflammatory, antihypertensive, anticoagulant, and especially had a good application prospect as anti-cancer drugs [20,21]. Lu et al. [22] designed and synthesized a novel compound containing benzimidazole structure that could inhibit tubulin. Studies have shown that compound **1** (Fig. 1) has a strong inhibitory effect on microtubule, with GI_{50} value of 30 nM and stable metabolism in human liver microsome with a half-life of 51 min. Wang's team [23] synthesized a series of 1-benzene acyl-2-(1-methylindol-3-yl)-benzimidazole derivatives. Compound **2** (Fig. 1) showed high activity and GI_{50} values were 2.4, 3.8 and 5.1 μM against A549, HepG2 and MCF-7 cell. Ahmed Kamal et al. [24] synthesized 20 arylpyrazole linked benzimidazole compounds. As a known pro-tubulin depolymerizer, Nocodazole [25] (Fig. 1) bound to the microtubule at the colchicine site although it had no structural similarity with colchicine. Benzimidazole was important in the structure of Nocodazole. On the basis of our previous research, we designed and synthesized a series of 1,2-diarylbenzimidazole derivatives (Fig. 1). The addition of benzimidazole structure to the microtubule inhibitor structure could increase both the structural stability and the bioactivity of the compound. The structure of the positive drug CA-4 was modified. The same 3,4,5-trimethoxy group as the ring A in the structure of CA-4 was designed, and the ring B was replaced differently. Only benzimidazole was used as the bridge to connect the ring A and ring B, and the two benzene rings were substituted at the 1 and 2 positions of benzimidazole, respectively. The synthetic methods and biological activities of these compounds were described in this paper. The binding modes of these compounds to tubulin were studied by *in vitro* cell experiment and computer simulation.

2. Results and discussion

2.1. Chemistry

The synthesis of compounds **c1-c24** (Table 1) followed the general method depicted in Scheme 1. *o*-Fluoronitrobenzene was refluxed with substituted aniline in water, neutralized with $NaHCO_3$, and then corresponding **a1-a5** were obtained and purified by silica gel column chromatography. Compounds **a1-a5** were dissolved in mixture solution (tetrahydrofuran and ethanol), and sodium dithionite solution was added for reduction reaction. After the alkalization by $NaHCO_3$, compounds **b1-b5** were obtained and purified by silica gel column chromatography. Compounds **b1-b5** were dissolved in anhydrous ethanol and then refluxed with substituted benzaldehyde to form imidazole ring. Recrystallized in ethanol system, **c1-c24** were obtained. All synthesized compounds **c1-c24** were determined by melting test, NMR, ESI-MS and elemental analysis, which were consistent with the depicted structures.

2.2. In vitro bioactivity assay

2.2.1. Inhibition of tubulin polymerization

The results for the *in vitro* tubulin polymerization inhibition of compounds **c1-c24** showed that compound **c24** exhibited the highest activity with IC_{50} (8.47 μM, Table 2). In the molecular structure of CA-4, the 3,4,5-trimethoxyl structure on A-ring was an essential condition for good activity. Eight compounds, **c1-c8**, were synthesized preliminarily to figure out which one of these R^1, R^2 rings functions better as A-ring. The substituents of R^2 ring in **c1-c4** were 3,4,5-trimethoxy, and R^1 ring mimicking the B-ring of CA-4 were non-substituent, 3-OH-4-OCH_3, 4-OCH_3 and 3-OH, respectively. Compounds **c5-c8** interchanged R^1 ring with R^2 ring of **c1-c4**. The IC_{50} value of **c1-c4** is bigger than that of **c5-c8**. Therefore, it is more appropriate to confirm that R^1 ring was A-ring, and the substituent group is 3,4,5-trimethoxy. According to the IC_{50} value, the activity was compared as follows: 3-Br < 2-Br < 4-Br (**c10** < **c11** < **c9**), 2-OCH_3 < 3-OCH_3 < 4-OCH_3 (**c13** < **c12** < **c7**). Two more groups of compounds were synthesized, including *meta*- and *para*-substitutions. Results of bioactivity comparison were as follows: 3-OH < 4-OH (**c8** < **c14**), 3-CH_3 < 4-CH_3 (**c16** < **c15**). Therefore, the *para*-substitutions could improve the activity of the compound more than that of the *ortho*-substitution and the *meta*-substitution. Four more *para*-substituted compounds were

Table 1

Structures of compounds **c1–c24**. 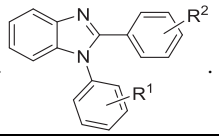

Compounds	R^1	R^2	Compounds	R^1	R^2
c1	H	3,4,5-$(OCH_3)_3$	**c13**	3,4,5-$(OCH_3)_3$	2-OCH_3
c2	3-OH-4-OCH_3	3,4,5-$(OCH_3)_3$	**c14**	3,4,5-$(OCH_3)_3$	4-OH
c3	4-OCH_3	3,4,5-$(OCH_3)_3$	**c15**	3,4,5-$(OCH_3)_3$	4-CH_3
c4	3-OH	3,4,5-$(OCH_3)_3$	**c16**	3,4,5-$(OCH_3)_3$	3-CH_3
c5	3,4,5-$(OCH_3)_3$	H	**c17**	3,4,5-$(OCH_3)_3$	4-SCH_3
c6	3,4,5-$(OCH_3)_3$	3-OH-4-OCH_3	**c18**	3,4,5-$(OCH_3)_3$	4-NO_2
c7	3,4,5-$(OCH_3)_3$	4-OCH_3	**c19**	3,4,5-$(OCH_3)_3$	4-F
c8	3,4,5-$(OCH_3)_3$	3-OH	**c20**	3,4,5-$(OCH_3)_3$	4-Cl
c9	3,4,5-$(OCH_3)_3$	4-Br	**c21**	3,4,5-$(OCH_3)_3$	2,4-$(OH)_2$
c10	3,4,5-$(OCH_3)_3$	3-Br	**c22**	3,4,5-$(OCH_3)_3$	3,4-$(OH)_2$
c11	3,4,5-$(OCH_3)_3$	2-Br	**c23**	3,4,5-$(OCH_3)_3$	2,4-$(OCH_3)_2$
c12	3,4,5-$(OCH_3)_3$	3-OCH_3	**c24**	3,4,5-$(OCH_3)_3$	3,4-$(OCH_3)_2$

synthesized in the hope of finding the most active substituents. In conclusion, the activity sequencing of different substituents was as follows: 4-SCH_3 < 4-NO_2 < 4-Cl < 4-Br < 4-F < 4-CH_3 < 4-OH < 4-OCH_3 (**c17** < **c18** < **c20** < **c8** < **c19** < **c15** < **c14** < **c7**). The effect of double substitution on activity was further considered. The substitutions of -OCH_3 and -OH with good activity were selected as substituents to synthesize *ortho-para* disubstituted compounds and *meta-para* disubstituted compounds respectively. 2,4-$(OH)_2$ < 3,4-$(OH)_2$ (**c21** < **c22**) and 2,4-$(OCH_3)_2$ < 3,4-$(OCH_3)_2$ (**c23** < **c24**). Therefore, the activity of *meta-para* disubstitution was superior to that of *ortho-para* disubstitution, in which 3,4-$(OCH_3)_2$ had the optimal activity.

2.2.2. Anti-proliferative activity

Anti-proliferative activity of compounds **c1-c24** on human cervical carcinoma (HeLa), human liver cancer cell (HepG2), human non-small cell lung carcinoma (A549), human breast cancer cell (MCF-7) was studied. The results were shown in Table 3. Among the 24 compounds, the anti-proliferative activity of compound **c24** was high, which was 1.71 μM, 0.71 μM, 2.41 μM and 1.94 μM against HeLa, HepG2, A549 and MCF-7 cells, respectively. R^1 ring with 3,4,5-trimethoxy was more active than R^2 ring with 3,4,5-trimethoxy. *Ortho*-substitution activity was poorer, followed by *meta*-substitution, and *para*-substitution activity was the highest. The activity of compounds with double substitution was better than that of a single substitution. In different cell lines, the structure-activity relationship was basically consistent with the description in 2.2.1, but there were still some differences, which may be due to different absorption capacity of the compounds. The MTT assay was performed on human normal liver cells (L02) to test the toxicity of the compounds. CC_{50} values were all above 100 μM, so the toxicity of the compounds was relatively weak.

Table 2
In vitro tubulin inhibitory activity of compound **c1-c24**.

Compounds	IC_{50} ± SD (μM)	Compounds	IC_{50} ± SD (μM)
c1	109.73 ± 3.05	**c13**	39.34 ± 0.53
c2	128.12 ± 3.46	**c14**	17.16 ± 0.41
c3	87.92 ± 2.11	**c15**	19.60 ± 0.29
c4	117.96 ± 1.59	**c16**	21.30 ± 0.37
c5	145.77 ± 2.36	**c17**	140.00 ± 2.08
c6	50.22 ± 0.78	**c18**	125.66 ± 2.01
c7	9.35 ± 0.13	**c19**	19.75 ± 0.64
c8	25.22 ± 0.44	**c20**	29.43 ± 0.71
c9	28.60 ± 0.57	**c21**	16.36 ± 0.52
c10	37.62 ± 0.62	**c22**	14.45 ± 0.39
c11	35.44 ± 0.55	**c23**	11.77 ± 0.28
c12	28.21 ± 0.42	**c24**	8.47 ± 0.11
CA-4	5.95 ± 0.07		

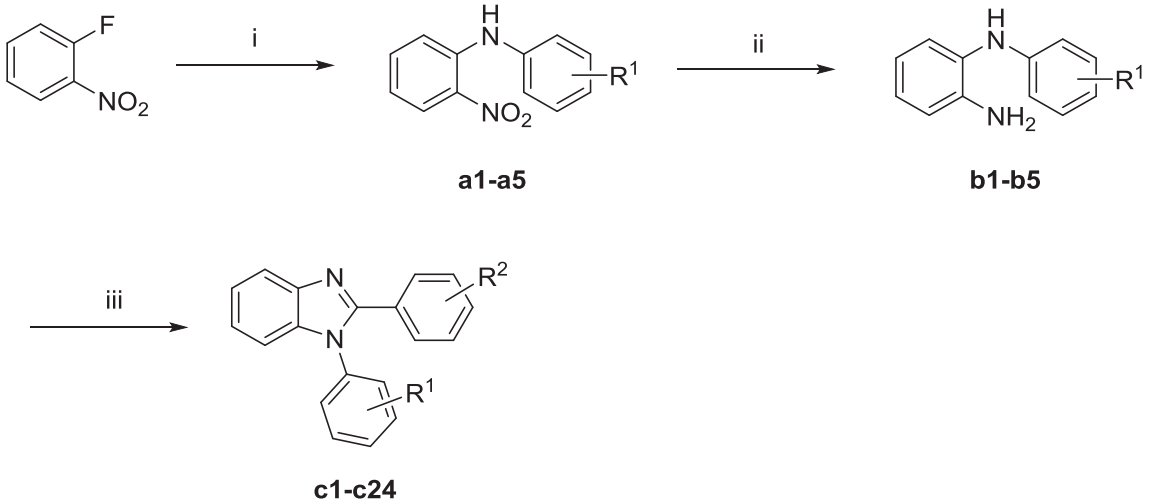

Scheme 1. General synthesis of compound **c1-c24**. Reagents and conditions: (i) substituted aniline, H_2O, reflux, 6 h; (ii) $Na_2S_2O_4$, THF/EtOH, 0 °C~r.t., 3 h; (iii) substituted benzaldehyde, EtOH, reflux, 3 h.

Table 3
In vitro antiproliferative activity and cytotoxicity of compound **c1-c24**.

Compounds	GI_{50} ± SD (μM)				CC_{50} ± SD (μM)
	HeLa	HepG2	A549	MCF-7	L02
c1	12.35 ± 1.22	11.72 ± 1.05	15.26 ± 1.41	13.94 ± 1.01	> 100
c2	11.43 ± 0.98	10.18 ± 1.02	14.63 ± 1.35	12.58 ± 1.11	> 100
c3	15.42 ± 0.99	10.44 ± 1.01	13.55 ± 1.13	12.16 ± 1.21	> 100
c4	12.32 ± 1.01	11.63 ± 1.09	16.41 ± 1.41	17.55 ± 1.67	> 100
c5	6.59 ± 0.59	9.48 ± 1.05	2.99 ± 0.28	15.49 ± 1.52	> 100
c6	10.75 ± 0.97	4.31 ± 0.31	13.39 ± 1.21	12.42 ± 1.15	> 100
c7	1.74 ± 0.15	0.93 ± 0.09	1.11 ± 0.08	1.37 ± 0.12	> 100
c8	3.37 ± 0.21	2.46 ± 0.20	3.38 ± 0.34	5.48 ± 0.47	> 100
c9	7.75 ± 0.76	2.08 ± 0.16	2.78 ± 0.21	5.11 ± 0.52	> 100
c10	12.96 ± 1.31	3.18 ± 0.30	10.04 ± 0.91	13.22 ± 1.08	> 100
c11	11.82 ± 1.15	4.22 ± 0.37	15.31 ± 1.36	13.19 ± 1.19	> 100
c12	2.78 ± 0.17	2.45 ± 0.13	2.74 ± 0.18	5.04 ± 0.61	> 100
c13	2.66 ± 0.13	3.35 ± 0.21	4.45 ± 0.19	5.39 ± 0.58	> 100
c14	3.11 ± 0.33	1.87 ± 0.16	4.78 ± 0.41	6.81 ± 0.72	> 100
c15	2.34 ± 0.13	1.96 ± 0.20	2.44 ± 0.22	4.27 ± 0.35	> 100
c16	1.69 ± 0.08	2.49 ± 0.16	1.75 ± 0.13	6.37 ± 0.54	> 100
c17	9.77 ± 0.96	8.87 ± 0.27	2.03 ± 0.18	10.41 ± 0.89	> 100
c18	13.42 ± 1.51	7.41 ± 0.71	12.71 ± 1.22	10.89 ± 0.95	> 100
c19	7.52 ± 0.67	2.32 ± 0.13	3.53 ± 0.27	6.58 ± 0.61	> 100
c20	6.85 ± 0.72	2.17 ± 0.19	9.04 ± 0.96	8.33 ± 0.91	> 100
c21	6.33 ± 0.71	1.69 ± 0.18	2.37 ± 0.21	4.02 ± 0.43	> 100
c22	4.23 ± 0.41	1.07 ± 0.11	3.97 ± 0.32	4.39 ± 0.51	> 100
c23	2.06 ± 0.17	0.84 ± 0.11	5.56 ± 0.53	3.29 ± 0.26	> 100
c24	1.71 ± 0.14	0.71 ± 0.07	2.41 ± 0.31	1.94 ± 0.08	> 100
CA-4	1.57 ± 0.52	0.65 ± 0.09	2.12 ± 0.61	1.21 ± 0.33	> 100

2.2.3. Cell cycle arrest

Tubulin inhibitors could inhibit the polymerization of tubulin and thus interfere with mitosis. Cell cycle assay was performed by PI staining to verify whether compound **c24** could prevent mitosis. HeLa and HepG2 cells were treated with 0.4, 0.8, 1.6, 2.4 and 3.2 μM **c24** for 24 h, respectively, forming a concentration gradient. Meanwhile, HeLa and HepG2 cells were treated with **c24** (0.8 μM) for gradient time (12 h, 24 h, 36 h and 48 h). It showed in Fig. 2 that compound **c24** caused cell cycle arrest into G2/M phase in concentration- and time-dependent manners. With the increase of concentration of **c24**, the percentage of cells in G2/M phase increased 2.5-fold as that of untreated cells. The rates of HepG2 cells in G2/M were 19.4%, 25.8%, 32.2%, 37.2%, and 49.2%, respectively, after 24 h of treatment with 0.4, 0.8, 1.6, 2.4 and 3.2 μM **c24**. When HepG2 cells were treated with 0.8 μM **c24** for 48 h, the percentage of cells in G2/M phase increased from 14.9% to 34.2%, compared with that untreated cells. The number of HeLa cells in G2/M phase also increased with the increase of time and concentration. Compared with untreated cells, the maximum number of HeLa cells in G2/M phase increased by 2–3 folds. As the concentration and time increased, the number of S-phase cells also increased, which may be due to gradual apoptosis after long-term or high-concentration. Compound **c24** had a similar effect on HeLa to HepG2. Therefore, compound **c24** could block the cell in G2/M phase and affect the normal mitosis of the cell.

2.2.4. Cellular reactive oxygen species accumulation

Acute high concentrations of reactive oxygen species (ROS) in cells could damage lipids, DNA and proteins in cells and disrupt normal cell function. Cancer cells had low clearance efficiency and higher sensitivity to ROS than normal cells. ROS was selectively harmful to cancer cells, which could be used in treatment. To verify whether **c24** could lead to the increase of intracellular ROS content, flow cytometry assay was performed with DCFH-DA staining. After the treatment of **c24**, there was a right-forward peak shift in the FL1-H, indicating that the content of intracellular ROS was increased in a time-dependent and concentration-dependent manner (Fig. 3). ROS increased in HeLa cells with the same trend. In conclusion, **c24** could lead to ROS accumulation in HeLa and HepG2 cells.

2.2.5. Cell apoptosis

Annexin V-FITC/PI assay was used to verify whether compound **c24** could induce apoptosis of cancer cells. HeLa and HepG2 cells were treated with 0.4, 0.8, 1.6, 2.4 and 3.2 μM **c24** for 24 h, respectively, to form a concentration gradient. Meanwhile, HeLa and HepG2 cells were treated with 0.8 μM **c24** for 12 h, 24 h, 36 h and 48 h, forming a time gradient. The percentage of FITC positive cells, namely the sum of early and late apoptotic cells, was used to represent the apoptotic rate. As shown in Fig. 4, the apoptotic rate of HepG2 cells was concentration- and time-dependent. With the increase of compound **c24** concentration, the apoptotic rate increased gradually up to 30%. Apoptotic cells were 20.85%, 22.87%, 26.66%, 28.16%, and 28.77%, respectively, after 24 h of treatment with 0.4, 0.8, 1.6, 2.4 and 3.2 μM **c24**. When cells were treated with the same concentration, apoptotic rate increased with the increase in treatment time. After 48 h of treatment, the apoptotic rate reached 25.88%, twice that of normal cells. Apoptotic rates of HepG2 cells treated by 0.8 μM **c24** at 12 h, 24 h, 36 h and 48 h were 14.32%, 15.92%, 16.82%, 20.09 and 25.88%, respectively. Compared with HepG2 cells, the apoptotic rate of HeLa cells treated by compound **c24** was similar. After treatment with 0.8 μM **c24** for 48 h and 3.2 μM **c24** for 24 h, the number of apoptotic cells was approximately twice that of untreated cells. Compound **c24** could also induce dose-dependent and time-dependent apoptosis of HeLa cells. In addition, an analysis of data from both cell lines showed that the treatment with the compound for a short period of time did not result in apoptosis or mild apoptosis. This indicated that after compound treatment, cancer cells firstly underwent mitotic arrest, which may lead to apoptosis. Therefore, compound **c24** could induce apoptosis of tumor cells, similar to other tubulin depolymerization agents.

2.2.6. Morphological effect of microtubule

The effect of the compound on microtubule was observed by immunofluorescence staining. Colchicine (0.5 μM), paclitaxel (0.5 μM) and compound **c24** (1.6 and 3.2 μM) were used to treat HepG2 and HeLa cells for 24 h, respectively. Microtubules were labeled with FITC, showing green under confocal microscopy, and nuclei were labeled with DAPI, showing blue. As shown in Fig. 5, microtubule in normal cultured cells was fibrous and clearly defined, and normal spindle shape

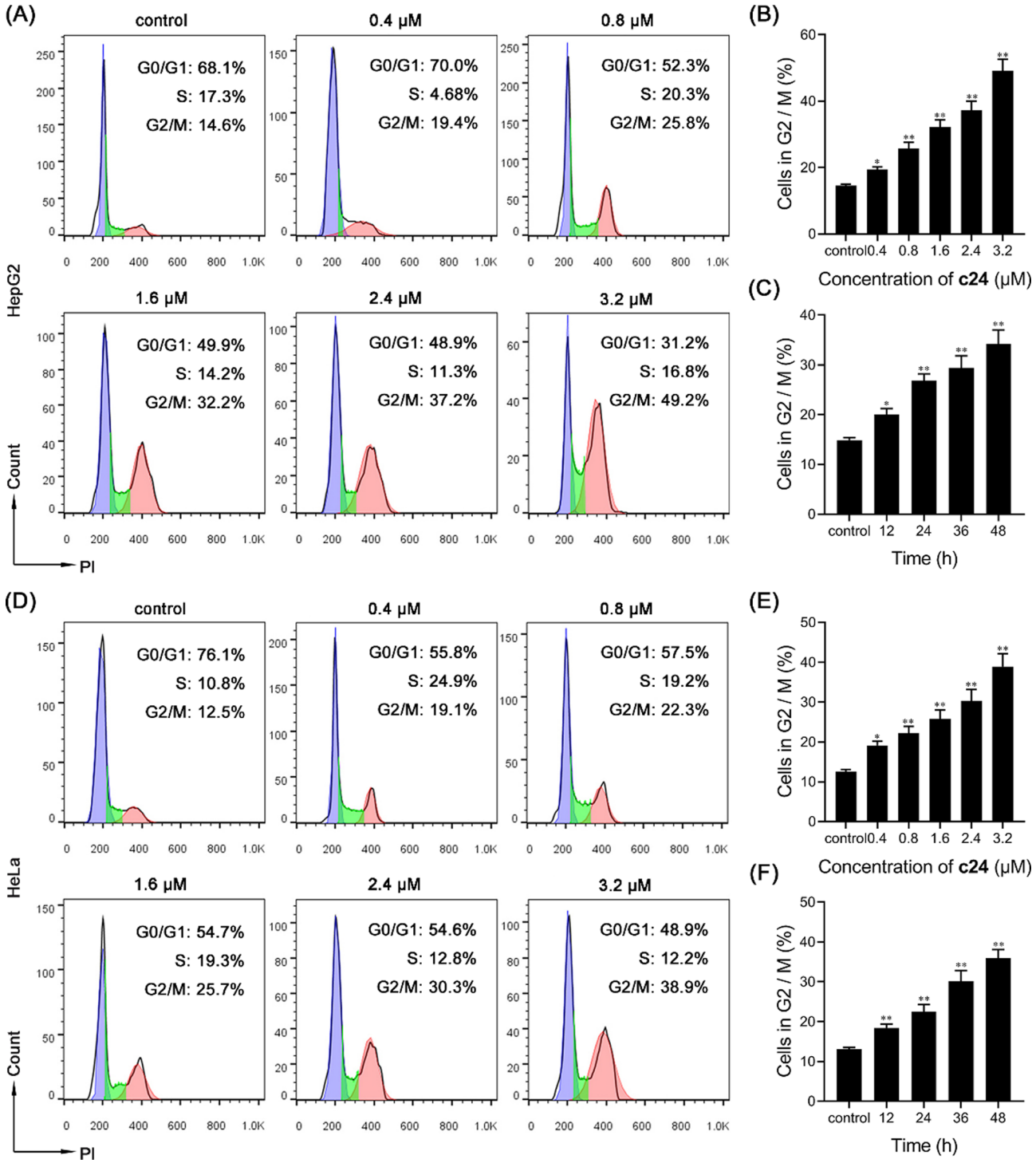

Fig. 2. Compound **c24** induced the cell cycle of HepG2 and HeLa arrest in the G2/M phase. Normal cultured cells were used as negative control (NC). (A and B) HepG2 cells were exposed to 0.4, 0.8, 1.6, 2.4 and 3.2 μM **c24** for 24 h. (C) HepG2 exposed to 0.8 μM **c24** for 12 h, 24 h, 36 h and 48 h. (D and E) HeLa cells were exposed to 0.4, 0.8, 1.6, 2.4 and 3.2 μM **c24** for 24 h. (F) HeLa were exposed to 0.8 μM **c24** for 12 h, 24 h, 36 h and 48 h. Cells were collected, stained with PI, and analyzed by flow cytometry. Data shown are representative of three independent experiments. $^{*}p < 0.05$, $^{**}p < 0.01$, $^{***}p < 0.001$ vs. control.

could be observed. Colchicine and paclitaxel could cause morphological changes and abnormalities of tubulin. Colchicine was a microtubule depolymerization agent, which could inhibit the polymerization of microtubule. Under confocal microscope, microtubule fibers were observed to become short and dispersed from slender fibrous shape. Paclitaxel was a promoter of tubulin polymerization, significantly enhancing the ability of tubulin polymerization, and then microtubule fibers became long and thick. After treatment with compound **c24**, the cells were normally elongated and rounded. After HepG2 and HeLa cells were treated by compound **c24**, the changes of microtubule fibers were similar to colchicine but different from paclitaxel. With the increase of compound **c24** concentration, the number of morphological changed or apoptotic cells increased. At the same time, some features of mitotic mutations, such as polykaryocyte and abnormal mitotic spindles, could be observed. The results showed that compound **c24** promoted the depolymerization of tubulin and affected the normal mitosis of cells.

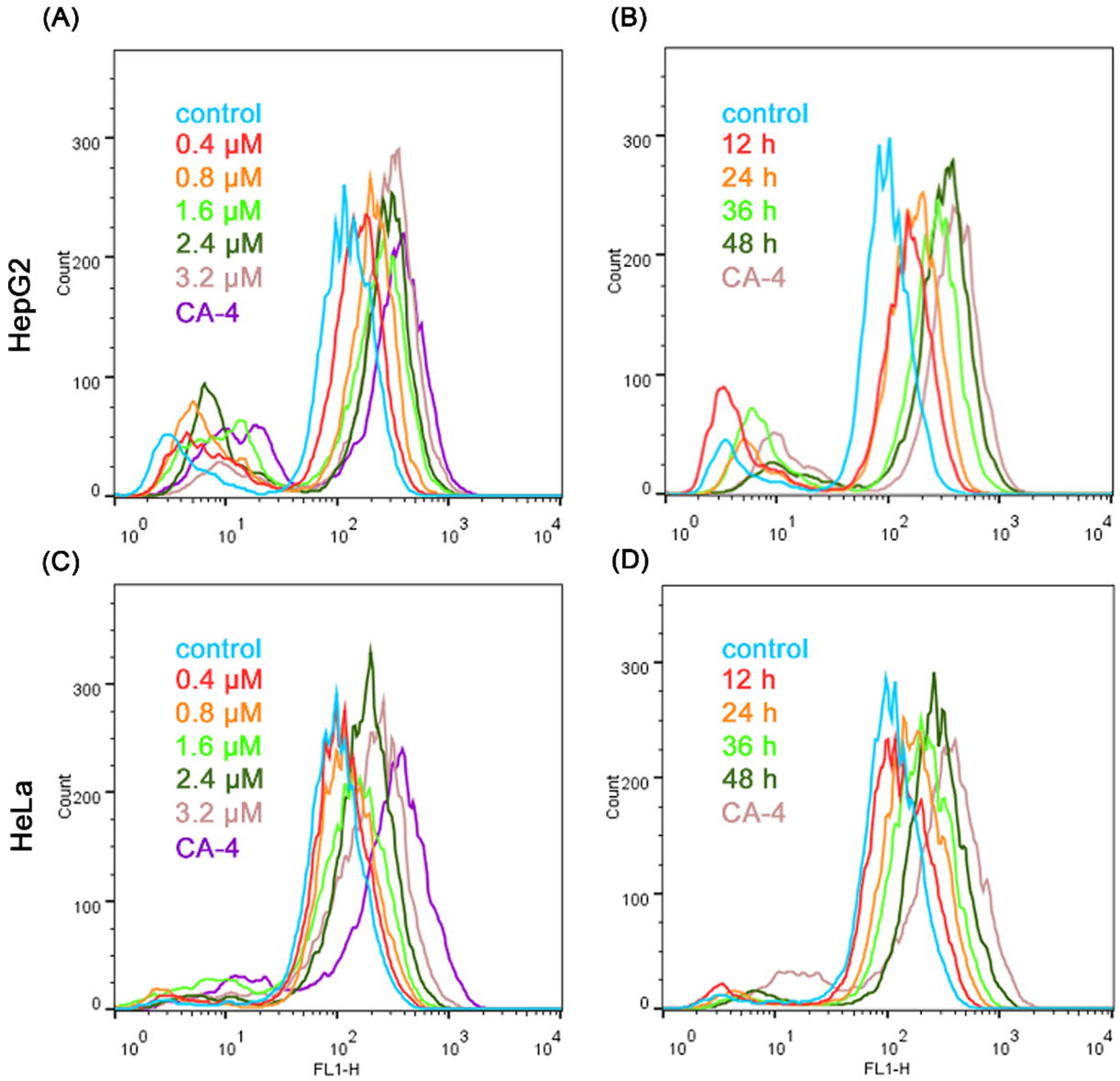

Fig. 3. Reactive oxygen species analysis of HepG2 and HeLa cells after compound **c24** treatment. Normal cultured cells were used as negative control (NC). CA-4 was treated as a positive agent. (A) HepG2 cells were exposed to 0.4, 0.8, 1.6, 2.4 and 3.2 μM **c24** for 24 h. (B) HepG2 cells exposed to 0.8 μM **c24** for 12 h, 24 h, 36 h and 48 h (C) HeLa cells were exposed to 0.4, 0.8, 1.6, 2.4 and 3.2 μM **c24** for 24 h. (D) HeLa cells were exposed to 0.8 μM **c24** for 12 h, 24 h, 36 h and 48 h. Cells were collected, stained with DCFH-DA, and analyzed by flow cytometry. Data shown are representative of three independent experiments.

2.3. Computational simulation

2.3.1. Molecular docking

Discovery Studio (DS, version 3.5) software was performed for molecular docking to simulate the binding ability and mode of compound **c1-c24** and tubulin. On the basis of the crystal complex of colchicine and microtubule protein (PDB ID: 1SA0 [26]), colchicine at the binding site of colchicine was replaced with compound **c1-c24**. Among them, the most effective compound **c24** showed the lowest interaction energy −50.72 kcal/mol, while the CDocker energy of positive drug CA-4 was −50.63 kcal/mol. The CDocker energy of compound **c24** and CA-4 are basically the same. Therefore, the binding ability of compound **c24** to colchicine binding sites is similar to that of positive drug CA-4. Fig. 6 showed the modes of colchicine, CA-4 and **c24** bound to tubulin.

There were many similarities between the binding of compound **c24** to tubulin and the positive drug. 3,4,5-Trimethoxybenzene was an important functional group of colchicine and CA-4 as microtubule inhibitors. The docking direction of **c24** was the same as that of the positive drug, especially the alignment of 3,4,5-trimethoxy. One of the 3,4,5-trimethoxy groups in colchicine was linked to the protein residues of tubulin (CYS B: 241) by a hydrogen bonding (distance = 1.98 Å) (Fig. 6**A and B**). Similarly, in CA-4, the 3,4,5-trimethoxy group was connected to the protein residue (CYS B: 241) by a hydrogen bond (distance = 2.31 Å) (Fig. 6**C and D**). This hydrogen bond was one of important interactions. The 3,4,5-trimethoxy group of **c24** was also linked to the protein residue (CYS B: 241) by hydrogen bonds (distance = 2.38 Å, Fig. 6**E and F**). Other functional groups of **c24** were connected to the microtubule protein in other ways, such as π-cation interactions. These bonds could ensure that **c24** bound tightly to tubulin. Meanwhile, 3,4,5-trimethoxyphenyl of **c24** was surrounded by hydrophobic residues such as leucine, isoleucine and valine.

2.3.2. 3D-QSAR model

Synthetic benzimidazole derivatives were analyzed by using the QSAR program built into the DS software to obtain the systematic SAR spectra as an anti-tubulin polymeric agent, so as to explore more

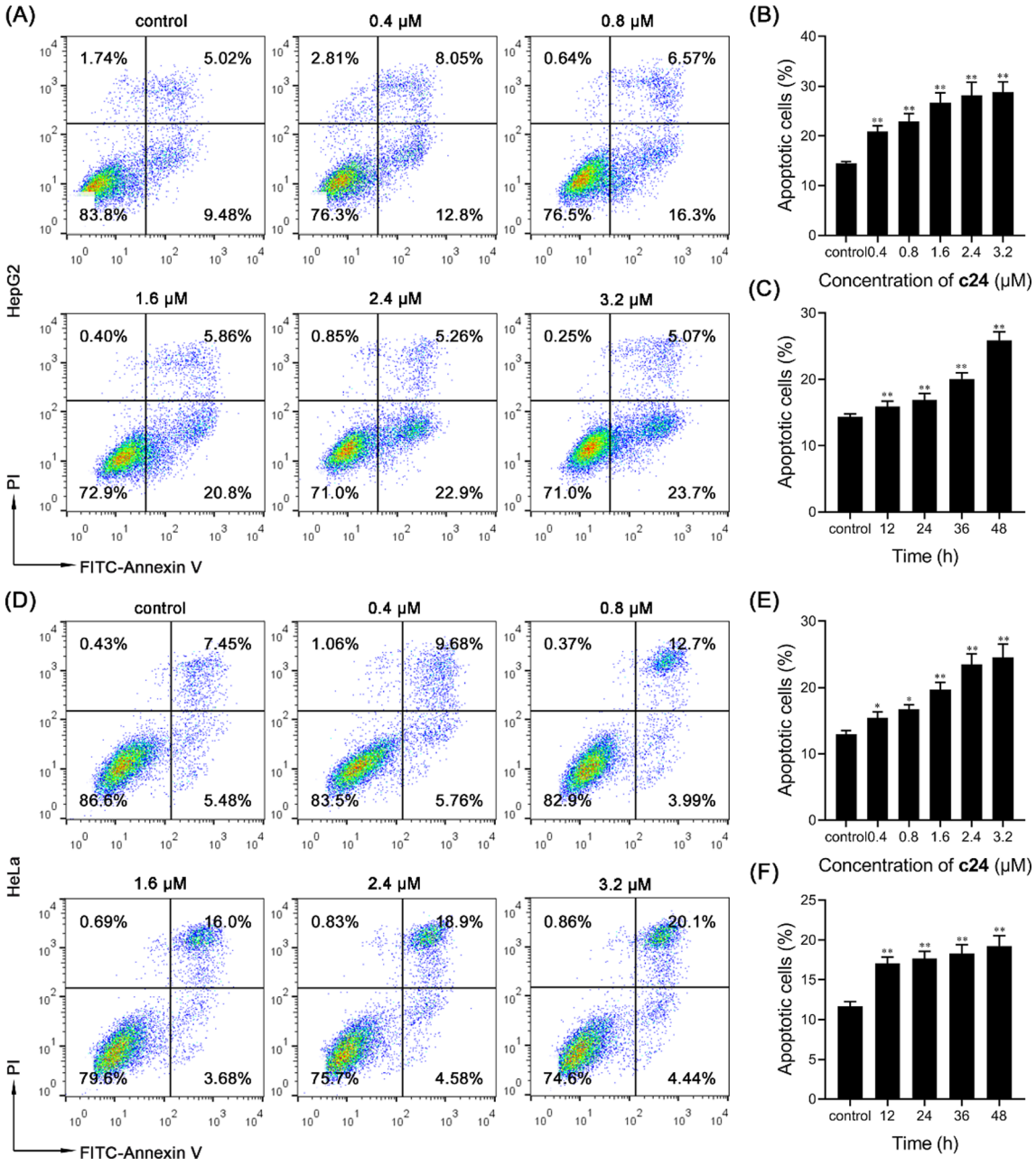

Fig. 4. Compound **c24** induced apoptosis of HepG2 and HeLa. Normal cultured cells were used as negative control (NC). (A and B) HepG2 cells were exposed to 0.4, 0.8, 1.6, 2.4 and 3.2 μM **c24** for 24 h. (C) HepG2 exposed to 0.8 μM **c24** for 12 h, 24 h, 36 h and 48 h. (D and E) HeLa cells were exposed to 0.4, 0.8, 1.6, 2.4 and 3.2 μM **c24** for 24 h. (F) HeLa were exposed to 0.8 μM **c24** for 12 h, 24 h, 36 h and 48 h. Cells were collected, stained with PI and FITC-Annexin V, and analyzed by flow cytometry. Data shown are representative of three independent experiments. $^{*}p < 0.05$, $^{**}p < 0.01$, $^{***}p < 0.001$ vs. control.

effective and more selective anti-tumor drugs. The IC_{50} value was converted into pIC_{50} value, and the training set and test set were randomly screened by the random multi-molecular method. The training set accounted for 83% of all compounds and the test set was the remaining four compounds. The difference between the converted pIC_{50} value and the predicted value by computer simulation was shown in Fig. 7. The R^2 value was 0.839, indicating a high degree of fitting between the calculated value and the predicted value. The 3D-QSAR model could also be used to predict the biological activity of benzimidazole derivatives.

All the molecules in the 3D-QSAR model are arranged on the electrostatic potential grid (Fig. 8**A**) and van der Waals force grid (Fig. 8**B**) in an isosurface manner. In the electrostatic potential grid, the red regions were regions of high electron density (negative charge), which was expected to decrease activity, and the blue regions were regions of low electron density (positive charge), which was expected to increase activity. In the van der Waals force grid, the green area refers to the area where the expected spatial volume will increase activity, and the yellow area refers to the area where the expected spatial volume will decrease activity. Good anti-tubulin polymerization agents should have a strong van der Waals force (green area) and strong polar groups (blue area). Based on the 3D-QSAR model, further structural modification of the compound could be carried out, laying a foundation for future research.

3. Conclusion

1,2-Diarylbenzimidazole derivatives were synthesized and their

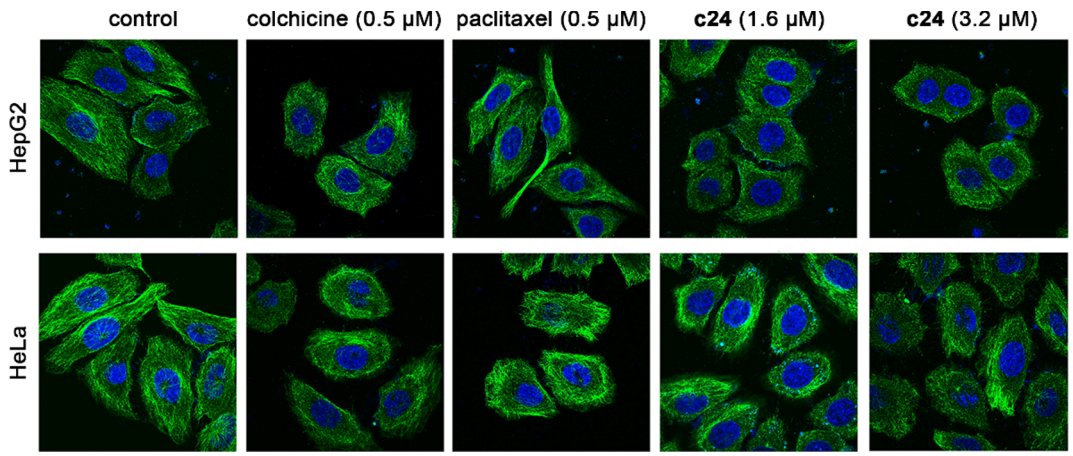

Fig. 5. Effects of colchicine (0.5 μM), paclitaxel (0.5 μM) and **c24** (1.6 μM and 3.2 μM) on microtubules in HepG2 and HeLa cells (tubulins, green; nuclei, blue.)

activities were evaluated. The compound showed good proliferation activity of anticancer cells *in vitro* in MTT assay. Among all compounds, **c24** showed the highest anti-proliferative activity, corresponding to HeLa, HepG2, A549 and MCF-7, and the IC_{50} values were 1.71, 0.71, 2.41 and 0.94 μM, respectively. The activity of anti-tubulin polymerization was well demonstrated in tubulin inhibition experiments. The microtubule inhibition value of **c24** was 8.47 μM. MTT assay of normal liver cells (L02) showed that the compounds were relatively less cytotoxic. Cell cycle tests showed that, like most tubulin inhibitors [27], compound **c24** could block tumor cells in G2/M phase, then affecting mitosis. In addition, confocal assay showed that **c24** promoted the depolymerization of tubulin, mitotic arrest, and formation of polykaryotic cells. According to the results of reactive oxygen species detection, it was observed that **c24** could effectively increase the content of reactive oxygen species in cells. Combined with the results of apoptosis assay, it was speculated that **c24** could promote apoptosis and might be related to the increase in the content of reactive oxygen species [28]. In addition, the possibility of **c24** binding to colchicine binding sites of tubulin was studied by computer simulation of molecular docking and the construction of 3D-QSAR model. Through the analysis of the binding model of compound **c24** to tubulin, it was observed that it had some strong interactions with protein, which might be helpful for its anti-microtubule polymerization. The study of the binding relationship between the compounds and tubulin was helpful for the further structural modification of the compounds and the development of more effective tubulin polymerization inhibitors.

4. Experimental

4.1. Chemistry general

All chemicals used were purchased from Aladdin (Shanghai, China). All reagents and solvents were of analytical or synthetic grade. Melting points were taken on an X4 MP apparatus (Jingsong Corp, Shanghai, China). All the ^{1}H NMR spectra were registered in DMSO-d_6 on Bruker AM 600 model spectrometer (Rhenistetten-Forchheim, Germany), operating at 600 MHz and using tetramethylsilane (TMS) as internal standard and DMSO as solvents. The progress of the reaction and purity of the products were checked on TLC plates coated with Merck silica gel 60 GF254, and the spots were visualized in UV light (254 nm and 365 nm). ESI-MS spectra were recorded on a Mariner System 5304 Mass spectrometer. Elemental analyses were performed on a CHN-O-Rapid instrument and were within 0.4% of the theoretical values.

4.1.1. General procedure for synthesis of **a1-a5**

o-Fluoronitrobenzene (14.10 g, 100 mmol) and 3,4,5-trimethoxyaniline (21.98 g, 120 mmol) were added into water (150 mL). The mixture was reflux for 6 h under stirring. Then the reaction complex was cooled to room temperature, neutralized with $NaHCO_3$, extracted with ethyl acetate, dried with anhydrous sodium sulfate, and vacuum evaporated to obtain the crude product of compound **a1**. Compound **a1** was purified by silica gel column chromatography. Compounds **a2-a5** were prepared by performing the method above.

4.1.2. General procedure for synthesis of **b1-b5**

In the ice bath conditions, a mixture of compound **a1** (6.09 g, 20.0 mmol) and anhydrous ethanol (50 mL) in tetrahydrofuran (100 mL) was added into sodium dithionite aqueous solution (55.71 g, 320 mmol). The mixture was stirred at room temperature for 3 h, then saturated $NaHCO_3$ solution and extracted with ethyl acetate. Collect the organic layer, wash with saturated $NaHCO_3$ solution, dry with anhydrous sodium sulfate and concentrate to obtain crude compound **b1**. Compounds **b2-b5** were prepared by performing the method above.

4.1.3. General procedure for synthesis of **c1-c24**

Compound **b5** (0.09 g, 0.5 mmol) was dissolved in anhydrous ethanol (5 mL), and 3,4,5-trimethoxybenzaldehyde (0.10 g, 0.5 mmol) was added. After stirring and refluxing for 3 h, solid crude products of compound **c1** were filtered and recrystallized in the ethanol system. Compounds **c2-c24** were prepared by performing the method above.

4.1.4. Structural characterization of compounds

*4.1.4.1. 3,4,5-Trimethoxy-N-(2-nitrophenyl)aniline (**a1**).* Orange powder (12.17 g, 40% yield), m.p. 182–183 °C. ^{1}H NMR (600 MHz, DMSO-d_6) δ 9.31 (s, 1H, -NH-), 8.11 (dd, J = 8.5, 1.5 Hz, 1H, Ar-H), 7.51 (t, J = 7.1 Hz, 1H, Ar-H), 7.24 (d, J = 8.1 Hz, 1H, Ar-H), 6.86 (t, J = 7.2 Hz, 1H, Ar-H), 6.68 (s, 2H, Ar-H), 3.76 (s, 6H, -OCH_3), 3.67 (s, 3H, -OCH_3). MS (ESI): 305.11 $[M + H]^+$; Anal. Calcd for $C_{15}H_{16}N_2O_5$: C, 59.21; H, 5.30; N, 9.21. Found: C, 59.07; H, 5.28; N, 9.23.

*4.1.4.2. N^1-(3,4,5-trimethoxyphenyl)benzene-1,2-diamine (**b1**).* Brown powder (3.29 g, 60% yield), m.p. 189–190 °C. ^{1}H NMR (600 MHz, DMSO-d_6) δ 7.01 (d, J = 7.0 Hz, 1H, Ar-H), 6.97 (s, 1H, -NH-), 6.81 (t, J = 7.0 Hz, 1H, Ar-H), 6.72 (d, J = 7.9 Hz, 1H, Ar-H), 6.54 (t, J = 7.5 Hz, 1H, Ar-H), 6.05 (s, 2H, Ar-H), 4.72 (s, 2H, -NH_2), 3.65 (s, 6H, -OCH_3), 3.56 (s, 3H, -OCH_3). MS (ESI): 275.13 $[M + H]^+$; Anal. Calcd for $C_{15}H_{18}N_2O_3$: C, 65.68; H, 6.61; N, 10.21. Found: C, 65.51; H, 6.59; N, 10.23.

*4.1.4.3. 1-Phenyl-2-(3,4,5-trimethoxyphenyl)-1H-benzo[d]imidazole (**c1**).* Yellow powder (0.14 g, 78% yield), m.p. 165–167 °C. ^{1}H NMR (600 MHz, DMSO-d_6) δ 7.70 – 7.40 (m, 5H, Ar-H), 7.10 – 6.93 (m, 4H, Ar-H), 6.77 (s, 1H, Ar-H), 6.50 (t, J = 7.2 Hz, 1H, Ar-H), 3.87 (s, 3H, -OCH_3), 3.71 (s, 3H, -OCH_3), 3.58 (s, 3H, -OCH_3). MS (ESI): 361.15

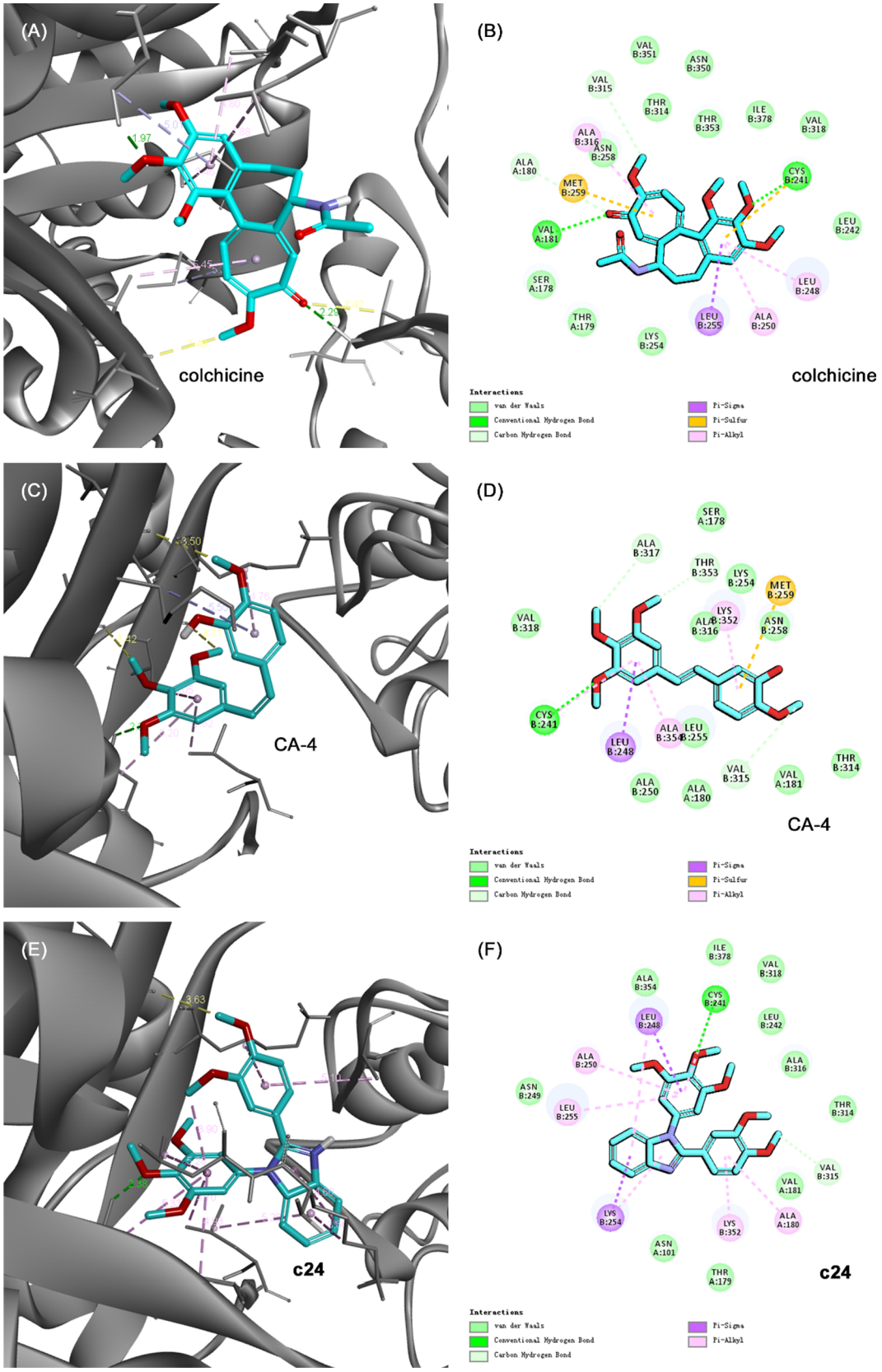

Fig. 6. The binding mode compound **c24** is in the colchicine binding site (CBS) of tubulin (PDB ID: 1SA0). In CBS and colchicine (A) or CA-4 (C) or compound **c24** (E) (The interactive 3D plots are shown separately between. Only the interacting residues are shown. Hydrogen bonds are shown as green dashed lines and π-cations are purple lines. A 2D plot of the interaction between CBS and colchicine (B) or CA-4 (D) or compound **c24** (F) is shown.

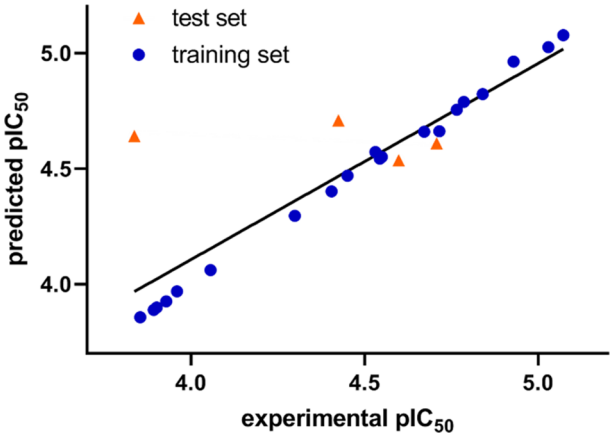

Fig. 7. Correlation between predicted pIC_{50} values of tubulin inhibitory activity and experimental values, with 4 test compounds (orange) and 20 training compounds (blue).

$[M + H]^+$; Anal. Calcd for $C_{22}H_{20}N_2O_3$: C, 73.32; H, 5.59; N, 7.77. Found: C, 73.57; H, 5.57; N, 7.75.

*4.1.4.4. 2-Methoxy-5-(2-(3,4,5-trimethoxyphenyl)-1H-benzo[d]imidazol-1-yl) phenol (**c2**).* White powder (0.13 g, 65% yield), m.p. 194–196 °C. ^{1}H NMR (600 MHz, DMSO-d_6) δ 8.56 (s, 1H, -OH), 7.96 (s, 1H, Ar-H), 6.69– 6.51 (m, 4H, Ar-H), 6.47 (t, J = 7.8 Hz, 2H, Ar-H), 6.05 (s, 1H, Ar-H), 5.69 (d, J = 1.2 Hz, 1H, Ar-H), 3.80 (s, 3H, -OCH_3), 3.66 (s, 3H, -OCH_3), 3.53 (s, 3H, -OCH_3), 3.36 (s, 3H, -OCH_3). ^{13}C NMR (151 MHz, DMSO-d_6) δ: 152.35, 149.01, 146.42, 140.07, 135.30, 133.58, 129.92, 126.24, 125.97, 121.11, 119.62, 116.13, 112.36, 110.09, 61.51, 57.05. MS (ESI): 407.15 $[M + H]^+$; Anal. Calcd for $C_{23}H_{22}N_2O_5$: C, 67.97; H, 5.46; N, 6.89. Found: C, 67.72; H, 5.48; N, 6.91.

*4.1.4.5. 1-(4-Methoxyphenyl)-2-(3,4,5-trimethoxyphenyl)-1H-benzo[d] imidazole (**c3**).* White powder (0.15 g, 77% yield), m.p. 171–173 °C. ^{1}H NMR (600 MHz, DMSO-d_6) δ 7.21 – 7.14 (m, 4H, Ar-H), 6.95 (s, 2H, Ar-H), 6.71 (s, 2H, Ar-H), 6.48 (s, 2H, Ar-H), 3.85 (s, 3H, -OCH_3), 3.76 (s, 3H, -OCH_3), 3.60 (s, 3H, -OCH_3), 3.51 (s, 3H, -OCH_3). MS (ESI): 391.16 $[M + H]^+$; Anal. Calcd for $C_{23}H_{22}N_2O_4$: C, 70.75; H, 5.68; N, 7.18. Found: C, 70.89; H, 5.67; N, 7.19.

*4.1.4.6. 3-(2-(3,4,5-Trimethoxyphenyl)-1H-benzo[d]imidazol-1-yl) phenol (**c4**).* White powder (0.14 g, 71% yield), m.p. 163–165 °C. ^{1}H NMR (600 MHz, DMSO-d_6) δ 9.13 (s, 1H, -OH), 7.09 – 6.98 (m, 4H, Ar-H), 6.72 (s, 1H, Ar-H), 6.65 (s, 1H, Ar-H), 6.63 (s, 1H, Ar-H), 6.60 (t, J = 2.4 Hz, 3H, Ar-H), 3.82 (s, 3H, -OCH_3), 3.69 (s, 3H, -OCH_3), 3.60 (s, 3H, -OCH_3). MS (ESI): 377.14 $[M + H]^+$; Anal. Calcd for $C_{22}H_{20}N_2O_4$: C, 70.20; H, 5.36; N, 7.44. Found: C, 70.15; H, 5.37; N, 7.45.

*4.1.4.7. 2-Phenyl-1-(3,4,5-trimethoxyphenyl)-1H-benzo[d]imidazole (**c5**).* White powder (0.15 g, 81% yield), m.p. 171–173 °C. ^{1}H NMR (600 MHz, DMSO-d_6) δ 7.23 – 7.15 (m, 6H, Ar-H), 6.95 (s, 2H, Ar-H), 6.68 (s, 1H, Ar-H), 6.58 (s, 1H, Ar-H), 6.27 (s, 1H, Ar-H), 3.85 (s, 3H, -OCH_3), 3.71 (s, 3H, -OCH_3), 3.60 (s, 3H, -OCH_3). MS (ESI): 361.15 $[M + H]^+$; Anal. Calcd for $C_{22}H_{20}N_2O_3$: C, 73.32; H, 5.59; N, 7.77. Found: C, 73.18; H, 5.57; N, 7.74.

*4.1.4.8. 2-Methoxy-5-(1-(3,4,5-trimethoxyphenyl)-1H-benzo[d]imidazol-2-yl) phenol (**c6**).* White powder (0.14 g, 67% yield), m.p. 191–193 °C. ^{1}H NMR (600 MHz, DMSO-d_6) δ 8.57 (s, 1H, -OH), 7.94 (s, 1H, Ar-H), 6.67 – 6.37 (m, 6H, Ar-H), 6.05 (d, J = 6.0 Hz, 1H, Ar-H), 5.62 (d, J = 6.0 Hz, 1H, Ar-H), 3.77 (s, 3H, -OCH_3), 3.66 (s, 3H, -OCH_3), 3.63 (s, 3H, -OCH_3), 3.55 (s, 3H, -OCH_3). ^{13}C NMR (151 MHz, DMSO-d_6) δ: 157.92, 153.96, 148.73, 142.89, 138.02, 132.49, 131.55, 128.76, 123.65, 120.31, 118.62, 117.07, 116.58, 111.22, 105.91, 60.68, 56.72. MS (ESI): 407.15 $[M + H]^+$; Anal. Calcd for $C_{23}H_{22}N_2O_5$: C, 67.97; H, 5.46; N, 6.89. Found: C, 68.13; H, 5.44; N, 6.87.

*4.1.4.9. 2-(4-Methoxyphenyl)-1-(3,4,5-trimethoxyphenyl)-1H-benzo[d] imidazole (**c7**).* White powder (0.14 g, 71% yield), m.p. 178–180 °C. ^{1}H NMR (600 MHz, DMSO-d_6) δ 7.13 – 7.01 (m, 5H, Ar-H), 6.73 – 6.70 (m, 3H, Ar-H), 6.61 (t, J = 7.0 Hz, 1H, Ar-H), 6.29 (s, 1H, Ar-H), 3.84 (s, 3H, -OCH_3), 3.69 (s, 3H, -OCH_3), 3.63 (s, 3H, -OCH_3), 3.57 (s, 3H, -OCH_3). ^{13}C NMR (151 MHz, DMSO-d_6) δ: 153.28, 149.69, 146.71, 142.07, 138.85, 131.96, 130.82, 126.91, 122.51, 119.13, 114.06, 108.58, 102.35, 61.02, 58.04. MS (ESI): 391.16 $[M + H]^+$; Anal. Calcd for $C_{23}H_{22}N_2O_4$: C, 70.75; H, 5.68; N, 7.18. Found: C, 70.92; H, 5.66; N, 7.16.

*4.1.4.10. 3-(1-(3,4,5-Trimethoxyphenyl)-1H-benzo[d]imidazol-2-yl) phenol (**c8**).* White powder (0.15 g, 80% yield), m.p. 172–174 °C. ^{1}H NMR (600 MHz, DMSO-d_6) δ 9.62 (s, 1H, -OH), 7.75 (t, J = 4.5 Hz, 1H, Ar-H), 7.31 – 6.80 (m, 7H, Ar-H), 6.75 (s, 2H, Ar-H), 3.75 (s, 3H, -OCH_3), 3.69 (s, 6H, -OCH_3). MS (ESI): 377.14 $[M + H]^+$; Anal. Calcd for $C_{22}H_{20}N_2O_4$: C, 70.20; H, 5.36; N, 7.44. Found: C, 70.41; H, 5.34; N, 7.45.

*4.1.4.11. 2-(4-Bromophenyl)-1-(3,4,5-trimethoxyphenyl)-1H-benzo[d] imidazole (**c9**).* White powder (0.16 g, 72% yield), m.p. 176–177 °C. ^{1}H

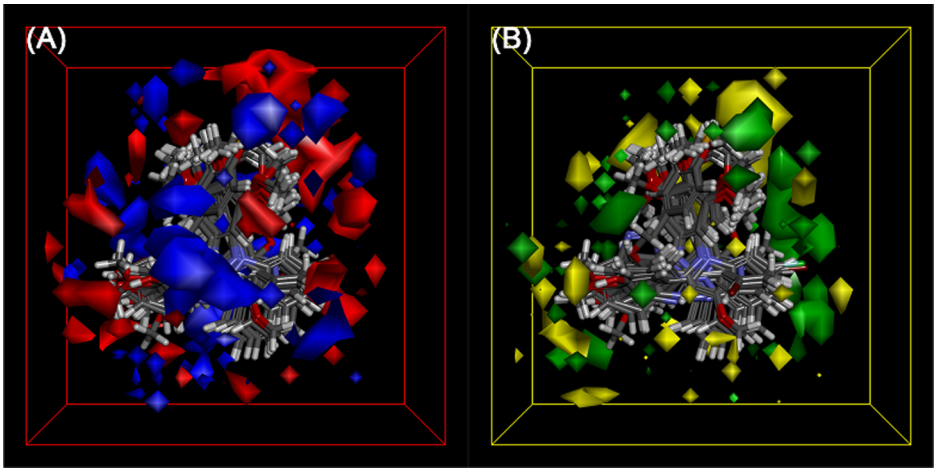

Fig. 8. (A) The isosurface of the coefficients on the electrostatic potential grid in the 3D-QSAR model. (B) The isosurface of the coefficients on the van der Waals grid in the 3D-QSAR model.

NMR (600 MHz, DMSO-d_6) δ 7.41 (d, J = 8.5 Hz, 2H, Ar-H), 7.18 (d, J = 8.4 Hz, 2H, Ar-H), 7.13 (s, 1H, Ar-H), 7.01 (s, 2H, Ar-H), 6.73 (s, 1H, Ar-H), 6.62 (t, J = 6.6 Hz, 1H, Ar-H), 6.28 (s, 1H, Ar-H), 3.84 (s, 3H, -OCH_3), 3.69 (s, 3H, -OCH_3), 3.60 (s, 3H, -OCH_3). MS (ESI): 439.06 $[M + H]^+$; Anal. Calcd for $C_{22}H_{19}BrN_2O_3$: C, 65.15; H, 4.36; N, 6.38. Found: C, 64.89; H, 4.35; N, 6.36.

*4.1.4.12. 2-(3-Bromophenyl)-1-(3,4,5-trimethoxyphenyl)-1H-benzo[d] imidazole (**c10**)*. White powder (0.19 g, 85% yield), m.p. 176–178 °C. ^{1}H NMR (600 MHz, DMSO-d_6) δ 7.23 – 7.10 (m, 5H, Ar-H), 6.96 (s, 2H, Ar-H), 6.51 (s, 1H, Ar-H), 6.40 (s, 1H, Ar-H), 6.22 (s, 1H, Ar-H), 3.81 (s, 3H, -OCH_3), 3.69 (s, 3H, -OCH_3), 3.60 (s, 3H, -OCH_3). MS (ESI): 439.06 $[M + H]^+$; Anal. Calcd for $C_{22}H_{19}BrN_2O_3$: C, 65.15; H, 4.36; N, 6.38. Found: C, 64.98; H, 4.37; N, 6.39.

*4.1.4.13. 2-(2-Bromophenyl)-1-(3,4,5-trimethoxyphenyl)-1H-benzo[d] imidazole (**c11**)*. White powder (0.19 g, 86% yield), m.p. 177–179 °C. ^{1}H NMR (600 MHz, DMSO-d_6) δ 7.52 (s, 1H, Ar-H), 7.41 (s, 3H, Ar-H), 7.18 (s, 2H, Ar-H), 7.13 (s, 1H, Ar-H), 6.91 (s, 1H, Ar-H), 6.73 (s, 1H, Ar-H), 6.61 (d, J = 6.0 Hz, 1H, Ar-H), 3.83 (s, 3H, -OCH_3), 3.70 (s, 3H, -OCH_3), 3.60 (s, 3H, -OCH_3). MS (ESI): 439.06 $[M + H]^+$; Anal. Calcd for $C_{22}H_{19}BrN_2O_3$: C, 65.15; H, 4.36; N, 6.38. Found: C, 65.38; H, 4.35; N, 6.36.

*4.1.4.14. 2-(3-Methoxyphenyl)-1-(3,4,5-trimethoxyphenyl)-1H-benzo[d] imidazole (**c12**)*. White powder (0.14 g, 72% yield), m.p. 179–181 °C. ^{1}H NMR (600 MHz, DMSO-d_6) δ 7.15 (s, 1H, Ar-H), 7.08 – 7.00 (m, 4H, Ar-H), 6.71 (t, J = 7.2 Hz, 2H, Ar-H), 6.64 – 6.59 (m, 2H, Ar-H), 6.30 (s, 1H, Ar-H), 3.84 (s, 3H, -OCH_3), 3.70 (s, 3H, -OCH_3), 3.64 (s, 3H, -OCH_3), 3.61 (s, 3H, OCH_3). MS (ESI): 391.16 $[M + H]^+$; Anal. Calcd for $C_{23}H_{22}N_2O_4$: C, 70.75; H, 5.68; N, 7.18. Found: C, 70.48; H, 5.67; N, 7.20.

*4.1.4.15. 2-(2-Methoxyphenyl)-1-(3,4,5-trimethoxyphenyl)-1H-benzo[d] imidazole (**c13**)*. White powder (0.14 g, 70% yield), m.p. 175–177 °C. ^{1}H NMR (600 MHz, DMSO-d_6) δ 7.62 (s, 2H, Ar-H), 7.08 – 7.00 (m, 3H, Ar-H), 6.71 (t, J = 7.2 Hz, 2H, Ar-H), 6.64 – 6.59 (m, 2H, Ar-H), 6.15 (s, 1H, Ar-H), 3.84 (s, 3H, -OCH_3), 3.70 (s, 3H, -OCH_3), 3.65 (s, 3H, -OCH_3), 3.59 (s, 3H, -OCH_3). MS (ESI): 391.16 $[M + H]^+$; Anal. Calcd for $C_{23}H_{22}N_2O_4$: C, 70.75; H, 5.68; N, 7.18. Found: C, 71.00; H, 5.69; N, 7.17.

*4.1.4.16. 4-(1-(3,4,5-Trimethoxyphenyl)-1H-benzo[d]imidazol-2-yl) phenol (**c14**)*. White powder (0.13 g, 70% yield), m.p. 164–166 °C. ^{1}H NMR (600 MHz, DMSO-d_6) δ 9.49 (s, 1H, -OH), 9.16 (s, 1H, Ar-H), 7.08 – 6.98 (m, 4H, Ar-H), 6.71 (s, 1H, Ar-H), 6.62 – 6.53 (m, 3H, Ar-H), 6.27 (s, 1H, Ar-H), 3.83 (s, 3H, -OCH_3), 3.68 (s, 3H, -OCH_3), 3.56 (s, 3H, -OCH_3). MS (ESI): 377.14 $[M + H]^+$; Anal. Calcd for $C_{22}H_{20}N_2O_4$: C, 70.20; H, 5.36; N, 7.44. Found: C, 70.41; H, 5.34; N, 7.42.

*4.1.4.17. 2-(p-Tolyl)-1-(3,4,5-trimethoxyphenyl)-1H-benzo[d]imidazole (**c15**)*. White powder (0.14 g, 77% yield), m.p. 184–186 °C. ^{1}H NMR (600 MHz, DMSO-d_6) δ 7.07 – 7.04 (m, 3H, Ar-H), 6.95 (d, J = 7.8 Hz, 1H, Ar-H), 6.90 (d, J = 7.8 Hz, 1H, Ar-H), 6.66 (s, 2H, Ar-H), 6.57 (s, 2H, Ar-H), 6.22 (s, 1H, Ar-H), 3.83 (s, 3H, -OCH_3), 3.69 (s, 3H, -OCH_3), 3.58 (s, 3H, -OCH_3), 2.15 (s, 3H, -CH_3). ^{13}C NMR (151 MHz, DMSO-d_6) δ: 152.33, 149.52, 146.41, 140.29, 137.54, 136.11, 134.96, 133.87, 124.01, 123.71, 120.86, 119.25, 115.61, 113.03, 111.55, 108.09, 61.51, 54.12, 21.49. MS (ESI): 375.16 $[M + H]^+$; Anal. Calcd for $C_{23}H_{22}N_2O_3$: C, 73.78; H, 5.92; N, 7.48. Found: C, 73.92; H, 5.90; N, 7.46.

*4.1.4.18. 2-(m-Tolyl)-1-(3,4,5-trimethoxyphenyl)-1H-benzo[d]imidazole (**c16**)*. White powder (0.14 g, 76% yield), m.p. 167–169 °C. ^{1}H NMR (600 MHz, DMSO-d_6) δ 7.27 – 7.03 (m, 2H, Ar-H), 7.00 (d, J = 1.2 Hz, 2H, Ar-H), 6.91 (s, 2H, Ar-H), 6.90 (s, 2H, Ar-H), 6.76 (s, 1H, Ar-H), 6.57 (s, 1H, Ar-H), 3.82 (s, 3H, -OCH_3), 3.68 (s, 3H, -OCH_3), 3.60 (s, 3H, -OCH_3), 2.14 (s, 3H, -CH_3). MS (ESI): 375.16 $[M + H]^+$; Anal. Calcd for $C_{23}H_{22}N_2O_3$: C, 73.78; H, 5.92; N, 7.48. Found: C, 73.79; H, 5.94; N, 7.47.

*4.1.4.19. 2-(4-(Methylthio)phenyl)-1-(3,4,5-trimethoxyphenyl)-1H-benzo [d]imidazole (**c17**)*. White powder (0.16 g, 81% yield), m.p. 187–189 °C. ^{1}H NMR (600 MHz, DMSO-d_6) δ 7.15 – 7.02 (m, 6H, Ar-H), 6.73 (s, 1H, Ar-H), 6.62 (t, J = 7.2 Hz, 2H, Ar-H), 6.30 (s, 1H, Ar-H), 3.84 (s, 3H, -OCH_3), 3.70 (s, 3H, -OCH_3), 3.59 (s, 3H, -OCH_3), 2.36 (s, 3H, -SCH_3). MS (ESI): 407.14 $[M + H]^+$; Anal. Calcd for $C_{23}H_{22}N_2O_3S$: C, 67.96; H, 5.46; N, 6.89. Found: C, 67.69; H, 5.44; N, 6.87.

*4.1.4.20. 2-(4-Nitrophenyl)-1-(3,4,5-trimethoxyphenyl)-1H-benzo[d] imidazole (**c18**)*. White powder (0.17 g, 83% yield), m.p. 170–172 °C. ^{1}H NMR (600 MHz, DMSO-d_6) δ 8.07 (d, J = 8.8 Hz, 2H, Ar-H), 7.40 (d, J = 4.7 Hz, 2H, Ar-H), 6.89 (s, 1H, Ar-H), 6.77 (s, 1H, Ar-H), 6.70 (s, 1H, Ar-H), 6.58 (s, 1H, Ar-H), 6.49 (s, 1H, Ar-H), 6.03 (s, 1H, Ar-H), 3.82 (s, 3H, -OCH_3), 3.68 (s, 3H, -OCH_3), 3.61 (s, 3H, -OCH_3). MS (ESI): 406.13 $[M + H]^+$; Anal. Calcd for $C_{22}H_{19}N_3O_5$: C, 65.18; H, 4.72; N, 10.37. Found: C, 65.39; H, 4.71; N, 10.33.

*4.1.4.21. 2-(4-Fluorophenyl)-1-(3,4,5-trimethoxyphenyl)-1H-benzo[d] imidazole (**c19**)*. White powder (0.14 g, 75% yield), m.p. 167–169 °C. ^{1}H NMR (600 MHz, DMSO-d_6) δ 7.23 (dd, J = 7.9, 5.6 Hz, 2H, Ar-H), 7.03 – 6.97 (m, 4H, Ar-H), 6.69 (s, 1H, Ar-H), 6.59 (t, J = 7.0 Hz, 2H, Ar-H), 6.28 (s, 1H, Ar-H), 3.82 (s, 3H, -OCH_3), 3.68 (s, 3H, -OCH_3), 3.58 (s, 3H, -OCH_3). ^{13}C NMR (151 MHz, DMSO-d_6) δ: 153.90, 149.13, 141.85, 138.16, 132.27, 126.27, 123.08, 118.37, 114.25, 106.44, 60.80, 57.10. MS (ESI): 379.14 $[M + H]^+$; Anal. Calcd for $C_{22}H_{19}FN_2O_3$: C, 69.83; H, 5.06; N, 7.40. Found: C, 69.62; H, 5.08; N, 7.09.

*4.1.4.22. 2-(4-Chlorophenyl)-1-(3,4,5-trimethoxyphenyl)-1H-benzo[d] imidazole (**c20**)*. White powder (0.14 g, 73% yield), m.p. 173–175 °C. ^{1}H NMR (600 MHz, DMSO-d_6) δ 7.26 – 7.23 (m, 4H, Ar-H), 7.10 (s, 1H, Ar-H), 7.00 (s, 2H, Ar-H), 6.71 (s, 1H, Ar-H), 6.61 (t, J = 6.6 Hz, 1H, Ar-H), 6.28 (s, 1H, Ar-H), 3.83 (s, 3H, -OCH_3), 3.69 (s, 3H, -OCH_3), 3.60 (s, 3H, -OCH_3). MS (ESI): 395.11 $[M + H]^+$; Anal. Calcd for $C_{22}H_{19}ClN_2O_3$: C, 66.92; H, 4.85; N, 7.09. Found: C, 67.15; H, 4.84; N, 7.08.

*4.1.4.23. 4-(1-(3,4,5-Trimethoxyphenyl)-1H-benzo[d]imidazol-2-yl) benzene-1,3-diol (**c21**)*. White powder (0.14 g, 73% yield), m.p. 183–185 °C. ^{1}H NMR (600 MHz, DMSO-d_6) δ 8.80 (s, 1H, -OH), 8.53 (s, 1H, -OH), 7.08 – 7.03 (m, 3H, Ar-H), 6.84 (s, 1H, Ar-H), 6.81 (s, 1H, Ar-H), 6.80 (s, 1H, Ar-H), 6.72 (s, 1H, Ar-H), 6.46 (s, 1H, Ar-H), 6.39 (s, 1H, Ar-H), 3.83 (s, 3H, -OCH_3), 3.71 (s, 3H, -OCH_3), 3.59 (s, 3H, -OCH_3). MS (ESI): 393.14 $[M + H]^+$; Anal. Calcd for $C_{22}H_{20}N_2O_5$: C, 67.34; H, 5.14; N, 7.14. Found: C, 67.26; H, 5.16; N, 7.12.

*4.1.4.24. 4-(1-(3,4,5-Trimethoxyphenyl)-1H-benzo[d]imidazol-2-yl) benzene-1,2-diol (**c22**)*. White powder (0.16 g, 81% yield), m.p. 189–191 °C. ^{1}H NMR (600 MHz, DMSO-d_6) δ 8.70 (s, 1H, -OH), 8.69 (s, 1H, -OH), 7.89 – 7.79 (m, 2H, Ar-H), 7.71 (d, J = 6.6 Hz, 1H, Ar-H), 7.64 – 7.41 (m, 3H, Ar-H), 7.10 (s, 1H, Ar-H), 6.94 (d, J = 8.6 Hz, 1H, Ar-H), 6.72 (t, J = 12.5 Hz, 1H, Ar-H), 3.76 (s, 3H, -OCH_3), 3.71 (s, 3H, -OCH_3), 3.59 (s, 3H, -OCH_3). MS (ESI): 393.14 $[M + H]^+$; Anal. Calcd for $C_{22}H_{20}N_2O_5$: C, 67.34; H, 5.14; N, 7.14. Found: C, 67.42; H, 5.12; N, 7.16.

*4.1.4.25. 2-(2,4-Dimethoxyphenyl)-1-(3,4,5-trimethoxyphenyl)-1H-benzo [d]imidazole (**c23**)*. White powder (0.14 g, 68% yield), m.p. 191–193 °C. ^{1}H NMR (600 MHz, DMSO-d_6) δ 7.41 (s, 1H, Ar-H), 7.00 (s, 1H, Ar-H), 6.94 (s, 1H, Ar-H), 6.74 (s, 1H, Ar-H), 6.61 (d, J = 2.3 Hz,

1H, Ar-H), 6.48 (d, J = 2.3 Hz, 1H, Ar-H), 6.32 – 6.29 (m, 1H, Ar-H), 6.27 (dd, J = 8.6, 2.3 Hz, 2H, Ar-H), 3.91 (s, 3H, -OCH_3), 3.80 (s, 3H, -OCH_3), 3.70 (s, 3H, -OCH_3), 3.61 (s 3H, -OCH_3), 3.59 (s 3H, -OCH_3). ^{13}C NMR (151 MHz, DMSO-d_6) δ: 152.49, 150.91, 146.24, 146.05, 140.55, 137.47, 136.67, 134.26, 133.62, 120.49, 120.12, 119.11, 118.73, 117.45, 115.62, 113.79, 111.77, 97.70, 61.24, 55.78. MS (ESI): 421.17 $[M + H]^+$; Anal. Calcd for $C_{24}H_{24}N_2O_5$: C, 68.56; H, 5.75; N, 6.66. Found: C, 68.81; H, 5.74; N, 6.65.

*4.1.4.26. 2-(3,4-Dimethoxyphenyl)-1-(3,4,5-trimethoxyphenyl)-1H-benzo [d]imidazole (**c24**)*. White powder (0.14 g, 67% yield), m.p. 190–192 °C. ^{1}H NMR (600 MHz, DMSO-d_6) δ 7.36 (d, J = 6.5 Hz, 1H, Ar-H), 7.23 – 7.17 (m, 1H, Ar-H), 7.08 – 7.01 (m, 2H, Ar-H), 6.72 – 6.62 (m, 3H, Ar-H), 6.33 (dd, J = 8.3, 1.9 Hz, 2H, Ar-H), 3.84 (d, J = 6.5 Hz, 3H, -OCH_3), 3.70 (s, 3H, -OCH_3), 3.67 (s, 3H, -OCH_3), 3.61 (d, J = 3.2 Hz, 6H, -OCH_3). ^{13}C NMR (151 MHz, DMSO-d_6) δ 157.57, 153.97, 152.33, 142.84, 137.88, 137.63, 132.59, 131.57, 129.76, 123.64, 123.05, 120.21, 119.66, 117.03, 116.45, 111.31, 105.74, 60.69, 56.62. MS (ESI): 421.17 $[M + H]^+$; Anal. Calcd for $C_{24}H_{24}N_2O_5$: C, 68.56; H, 5.75; N, 6.66. Found: C, 68.31; H, 5.73; N, 6.67.

4.2. Biological assays

4.2.1. MTT assay

Human cervical carcinoma (HeLa), human liver cancer cell (HepG2), human non-small cell lung carcinoma (A549), human breast cancer cell (MCF-7) and human normal liver cells (L02) were cultured in DMEM containing 10% fetal bovine serum (FBS) and 1% Penicillin-Streptomycin in 5% CO_2 atmosphere at 37 °C. Seed the cells in the logarithmic phase into 96-well plates (5000–10,000 cells per well). After 8–12 h, the compounds of various concentration (0.01, 0.1, 1, 10 and 100 μM) were added into the 96-wells plates. After 48 h, 10 μL MTT (5 mg mL^{-1}) were added to each well to incubate 4 h. Then discard the media and add DMSO (150 μL) to dissolve formazan completely on a shaker for 10 min. The absorbance was measured at 570 nm wavelength by microplate reader (Tecan, Switzerland). Three replicate wells were used for each concentration and each independent experiment was conducted at least three times. The GI_{50} was the compound concentration required to inhibit cell proliferation by 50% and the CC_{50} was the compound concentration to cause cytotoxic by 50%.

4.2.2. Tubulin polymerization assay

Microtubule was purified from fresh pig brain according to the previous method [29] with modification. Compounds of various concentrations (from 0.1 to 50 μM) were plated into 96-well plates (10 μL/well). Purified tubulin in G-PEM buffer was prepared freshly on ice and added into plates. Then the mixture was monitored by microplate reader at 350 nm at 37 °C. IC_{50} value was the concentration of the compound when the inhibitory rate of microtubule assembly by 50% after incubation for 20 min.

4.2.3. Cell cycle analysis

Cells were seeded into the 6-well plate (500,000 cells/mL) and treated with compound **c24** under various conditions (concentration and time) respectively. Then cells were collected, washed twice on ice and fixed with 70% ethanol at 4 °C overnight. Centrifugate and discard the supernatant. Cells were treated with RNAse (100 μL) for 30 min and stained with 400 μL PI in dark. The samples were tested on BD Accuri C6 flow cytometry (BD, USA) and the data was analyzed with Flowjo 7.6.1 (FlowJo, USA).

4.2.4. Reactive oxygen detection

Cells were seeded into the 6-well plate (500,000 cells/mL) and treated with compound **c24** under various conditions (concentration and time) respectively. Then cells were collected, washed twice on ice and stained with 1 mL of DCFH-DA solution (in DMEM) for 20 min in the cell incubator at 37 °C. Then cells were collected and washed twice with fresh DMEM. The samples were tested on BD Accuri C6 flow cytometry (BD, USA) and the data was analyzed with Flowjo 7.6.1 (FlowJo, USA).

4.2.5. Cell apoptosis assay

Cells were seeded into the 6-well plate (500,000 cells/mL) and treated with compound **c24** under various conditions (concentration and time) respectively. Cells were collected, washed twice on ice and resuspended in 500 μL staining buffer. Then it was stained with 5 μL AnnexinV-FITC and 5 μL PI in dark for 10 min. The samples were tested on BD Accuri C6 flow cytometry (BD, USA) and the data was analyzed with Flowjo 7.6.1 (FlowJo, USA).

4.2.6. Immunofluorescence

Cells were seeded into the 6-well plate (500,000 cells/mL) in which a glass cover was pre-positioned, and treated with compounds under various conditions (concentration and time) respectively. Cells were uniformly distributed in six-well plates with glass covers. After treatment, cells were fixed with fixed with 4% paraformaldehyde for 0.5–1 h, washed with PBS. After permeated with 1% Triton X-100 solution for 30 min, cells were incubated with immune dyeing sealing for 1 h. Then cells were incubated with Alexa Fluor 488 labeled tubulin antibody (1:500) at 4 °C overnight in the dark. Then cells were washed and stained by DAPI for 10 min, avoiding light. The cover glasses were fixed with anti-fluorescence quenching agent on the glass slide. Images were collected using the confocal laser scanning microscope (Olympus, Japan) and processed in Photoshop (Adobe, USA).

4.3. Docking simulations

The software Discovery Studio (version 3.5) was used to optimize the molecular structure and microtubule protein, and DS-CDOCKER was selected for simulated docking. Compound **c24** and positive drug CA-4 molecules were simulated in the three-dimensional X-ray structure (PDB ID: 1SA0) of the microtubule protein. The whole tubulin complex was defined as the receptor, and the interaction site was selected according to the binding position of colchicine ligand (CN2700). During the molecular docking process, the CN2700 molecule was removed and replaced by **c24**. All binding water and ligands in the docking results were removed from the protein and labeled with polar hydrogen. The types of interactions between proteins and ligands were analyzed, and the different binding bonds were labeled.

4.4. 3D-QSAR modeling

Using the software Discovery Studio (version 3.5), the ligand-based 3D-QSAR method was used for processing. The IC_{50} value of the inhibitory protein was converted to obtain the corresponding pIC_{50} value. All definitions of descriptors could be observed with the help of DS 3.5 software and they were calculated by QSAR protocol of DS 3.5. The coordination conformation of each molecule selects the CDOCKER result with the lowest interaction energy. The results of 3D-QSAR modeling can be evaluated according to the correlation coefficient of cross-validation. The random correlation risk was tested by scrambling (Y scrambling). The ability of the compound to inhibit tubulin was randomly reordered 20 times, and leave-one-out verification test was conducted respectively. The 3D-QSAR model was also verified by the test set, in which the compounds were not included in the training set.

Acknowledgement

This work was supported by the Public Science and Technology Research Funds Projects of Ocean (State Oceanic Administration, People's Republic of China, No. 201505023).

References

[1] B. Ahmad, S. Nawaz, S. Ali, S. Bashir, N. Mahmood, B. Gul, Level and evaluation of tumor marker CA-125 in ovarian cancer patients in Khyber Pakhtunkhwa, Pakistan, Asian Pacific J. Cancer Prev. 16 (2015) 185–189, https://doi.org/10.7314/APJCP.2015.16.1.185.

[2] X. Zhang, H. Zhang, Chemotherapy drugs induce pyroptosis through caspase-3-dependent cleavage of GSDME, Sci. China Life Sci. 61 (2018) 739–740, https://doi.org/10.1007/s11427-017-9158-x.

[3] K. Romanidis, E.-A. Nagorni, E. Halkia, M. Pitiakoudis, The role of cytoreductive surgery in advanced ovarian cancer: the general surgeon's perspective, Management 7 (2014) 12.

[4] R.Y. Zang, Z.T. Li, Z.Y. Zhang, S.M. Cai, Surgery and salvage chemotherapy for Chinese women with recurrent advanced epithelial ovarian carcinoma: a retrospective case-control study, Int. J. Gynecol. Cancer 13 (2003) 419–427, https://doi.org/10.1046/j.1525-1438.2003.13315.x.

[5] F.L. Marlow, Recent advances in understanding oogenesis: interactions with the cytoskeleton, microtubule organization, and meiotic spindle assembly in oocytes, F1000Research 7 (2018) 468, https://doi.org/10.12688/f1000research.13837.1.

[6] B.V. Kumbhar, D. Panda, A. Kunwar, Interaction of microtubule depolymerizing agent indanocine with different human aαβ tubulin isotypes, PLoS One 13 (2018) 1–20, https://doi.org/10.1371/journal.pone.0194934.

[7] M. Hemmat, B.T. Castle, D.J. Odde, Microtubule dynamics: moving toward a multi-scale approach, Curr. Opin. Cell Biol. 50 (2018) 8–13, https://doi.org/10.1016/j.ceb.2017.12.013.

[8] B.H. Choi, S. Chattopadhaya, L.N. Thanh, L. Feng, Q.T. Nguyen, C.B. Lim, A. Harikishore, R.P. Reddy, N. Bharatham, Y. Zhao, X. Liu, H.S. Yoon, Suprafenacine, an Indazole-hydrazide agent, target cancer cells through microtubule destabilization, PLoS One 9 (2014), https://doi.org/10.1371/journal.pone.0110955.

[9] X. Huang, R. Huang, Z. Wang, L. Li, S. Gou, Z. Liao, H. Wang, Pt(IV) complexes conjugating with chalcone analogue as inhibitors of microtubule polymerization exhibited selective inhibition in human cancer cells, Eur. J. Med. Chem. 146 (2018) 435–450, https://doi.org/10.1016/j.ejmech.2018.01.075.

[10] S. Banerjee, K.E. Arnst, Y. Wang, G. Kumar, S. Deng, L. Yang, G.B. Li, J. Yang, S.W. White, W. Li, D.D. Miller, Heterocyclic-fused pyrimidines as novel tubulin polymerization inhibitors targeting the colchicine binding site: structural basis and antitumor efficacy, J. Med. Chem. 61 (2018) 1704–1718, https://doi.org/10.1021/acs.jmedchem.7b01858.

[11] W. Yan, T. Yang, J. Yang, T. Wang, Y. Yu, Y. Wang, Q. Chen, P. Bai, D. Li, H. Ye, Q. Qiu, Y. Zhou, Y. Hu, S. Yang, Y. Wei, W. Li, L. Chen, SKLB060 reversibly binds to colchicine site of tubulin and possesses efficacy in multidrug-resistant cell lines, Cell. Physiol. Biochem. 47 (2018) 489–504, https://doi.org/10.1159/000489983.

[12] S.R. Punganuru, H.R. Madala, C.M. Mikelis, A. Dixit, V. Arutla, K.S. Srivenugopal, Conception, synthesis, and characterization of a rofecoxib-combretastatin hybrid drug with potent cyclooxygenase-2 (COX-2) inhibiting and microtubule disrupting activities in colon cancer cell culture and xenograft models, Oncotarget 9 (2018) 26109–26129, https://doi.org/10.18632/oncotarget.25450.

[13] P. Zhou, Y. Liang, H. Zhang, H. Jiang, K. Feng, P. Xu, J. Wang, X. Wang, K. Ding, C. Luo, M. Liu, Y. Wang, Design, synthesis, biological evaluation and cocrystal structures with tubulin of chiral β-lactam bridged combretastatin A-4 analogues as potent antitumor agents, Eur. J. Med. Chem. 144 (2018) 817–842, https://doi.org/10.1016/j.ejmech.2017.12.004.

[14] N.R. Penthala, H. Zong, A. Ketkar, N.R. Madadi, V. Janganati, R.L. Eoff, M.L. Guzman, P.A. Crooks, Synthesis, anticancer activity and molecular docking studies on a series of heterocyclic trans-cyanocombretastatin analogues as anti-tubulin agents, Eur. J. Med. Chem. 92 (2015) 212–220, https://doi.org/10.1016/j.ejmech.2014.12.050.

[15] N. Hura, A. Naaz, S.S. Prassanawar, S.K. Guchhait, D. Panda, Drug-clinical agent molecular hybrid: synthesis of diaryl(trifluoromethyl)pyrazoles as tubulin targeting anticancer agents, ACS Omega 3 (2018) 1955–1969, https://doi.org/10.1021/acsomega.7b01784.

[16] Y. Liu, D. Yang, Z. Hong, S. Guo, M. Liu, D. Zuo, D. Ge, M. Qin, D. Sun, Synthesis and biological evaluation of 4,6-diphenyl-2-(1H-pyrrol-1-yl)nicotinonitrile analogues of crolibulin and combretastatin A-4, Eur. J. Med. Chem. 146 (2018) 185–193, https://doi.org/10.1016/j.ejmech.2018.01.052.

[17] M. Mustafa, D. Abdelhamid, E.S.M.N. Abdelhafez, M.A.A. Ibrahim, A.M. Gamal-Eldeen, O.M. Aly, Synthesis, antiproliferative, anti-tubulin activity, and docking study of new 1,2,4-triazoles as potential combretastatin analogues, Eur. J. Med. Chem. 141 (2017) 293–305, https://doi.org/10.1016/j.ejmech.2017.09.063.

[18] S. Elmeligie, A.T. Taher, N.A. Khalil, A.H. El-said, Synthesis and cytotoxic activity of certain trisubstituted azetidin-2-one derivatives as a cis-restricted combretastatin A-4 analogues, Arch. Pharm. Res. 40 (2017) 13–24, https://doi.org/10.1007/s12272-016-0849-y.

[19] Z. Liu, Y. Chen, P. Liu, J. Wang, M. Huang, Cadmium(II) and cobalt(II) complexes generated from benzimidazole-5-carboxylate: self-assembly by hydrogen bonding and π-π Interactions, J. Solid State Chem. 178 (2005) 2306–2312, https://doi.org/10.1016/j.jssc.2005.04.037.

[20] R. Abraham, P. Prakash, K. Mahendran, M. Ramanathan, A novel series of N-acyl substituted indole-linked benzimidazoles and naphthoimidazoles as potential anti inflammatory, anti biofilm and anti microbial agents, Microb. Pathog. 114 (2018) 409–413, https://doi.org/10.1016/j.micpath.2017.12.021.

[21] A. Ravindernath, M.S. Reddy, Synthesis and evaluation of anti-inflammatory, antioxidant and antimicrobial activities of densely functionalized novel benzo [d] imidazolyl tetrahydropyridine carboxylates, Arab. J. Chem. 10 (2017) S1172–S1179, https://doi.org/10.1016/j.arabjc.2013.02.011.

[22] Y. Lu, J. Chen, J. Wang, C.M. Li, S. Ahn, C.M. Barrett, J.T. Dalton, W. Li, D.D. Miller, Design, synthesis, and biological evaluation of stable colchicine binding site tubulin inhibitors as potential anticancer agents, J. Med. Chem. 57 (2014) 7355–7366, https://doi.org/10.1021/jm500764v.

[23] Y.T. Wang, Y.J. Qin, N. Yang, Y.L. Zhang, C.H. Liu, H.L. Zhu, Synthesis, biological evaluation, and molecular docking studies of novel 1-benzene acyl-2-(1-methylindol-3-yl)-benzimidazole derivatives as potential tubulin polymerization inhibitors, Eur. J. Med. Chem. 99 (2015) 125–137, https://doi.org/10.1016/j.ejmech.2015.05.021.

[24] A. Kamal, T. Srinivasa Reddy, S. Polepalli, N. Shalini, V.G. Reddy, A.V. Subba Rao, N. Jain, N. Shankaraiah, Synthesis and biological evaluation of podophyllotoxin congeners as tubulin polymerization inhibitors, Bioorg. Med. Chem. 22 (2014) 5466–5475, https://doi.org/10.1016/j.bmc.2014.07.031.

[25] S. Sharma, B. Poliks, C. Chiauzzi, R. Ravindra, A.R. Blanden, S. Bane, Colchicine binding site on avian tubulin isotype βVI, Biochemistry 49 (2010) 2932–2942, https://doi.org/10.1021/bi100159p.

[26] R.B.G. Ravelli, B. Gigant, P.A. Curmi, I. Jourdain, S. Lachkar, A. Sobel, M. Knossow, Insight into tubulin regulation from a complex with colchicine and a stathmin-like domain, Nature 428 (2004) 198–202, https://doi.org/10.1038/nature02393.

[27] N.M. O'Boyle, M. Carr, L.M. Greene, O. Bergin, S.M. Nathwani, T. McCabe, D.G. Lloyd, D.M. Zisterer, M.J. Meegan, Synthesis and evaluation of azetidinone analogues of combretastatin A-4 as tubulin targeting agents, J. Med. Chem. 53 (2010) 8569–8584, https://doi.org/10.1021/jm101115u.

[28] G. Aziz, K. Odlo, T.V. Hansen, R.E. Paulsen, G.H. Mathisen, Combretastatin A-4 and structurally related triazole analogues induce caspase-3 and reactive oxygen species-dependent cell death in PC12 cells, Eur. J. Pharmacol. 703 (2013) 25–32, https://doi.org/10.1016/j.ejphar.2013.01.043.

[29] C. Gell, C.T. Friel, B. Borgonovo, D.N. Drechsel, A.A. Hyman, J. Howard, Purification of Tubulin from Porcine Brain, in: A. Straube (Ed.), Microtubule Dyn. Humana Press, Totowa, NJ, 2011, pp. 15–28, , https://doi.org/10.1007/978-1-61779-252-6.